INORGANIC CHEMISTRY FRONTIERS

RESEARCH ARTICLE

View Article Online
View Journal | View Issue

Cite this: *Inorg. Chem. Front.*, 2023, **10**, 7222

Zero-dimensional mixed-cation hybrid lead halides with broadband emissions†

Mirosław Mączka, * Dawid Drozdowski, Dagmara Stefańska and Anna Gągor

Zero-dimensional (0D) metal halides have received significant attention in recent years due to their attractive light-emitting properties derived from the presence of isolated building units. Here we report the synthesis, crystal structures, and linear optical and phonon properties of three newcomers to the family of 0D lead halides – $Cs_2MHy_2PbBr_6$, $Cs_2MHy_2PbI_6$ and $Cs_2MHy_2PbBr_3I_3$ (MHy^+ = methylhydrazinium) which are the first examples of 0D lead halides with mixed cations. These compounds crystallize in the orthorhombic *Cmce* structure with isolated PbX_6^{4-} octahedral units and statistically disordered MHy^+ cations. X-ray diffraction revealed the selective substitution of halide ions in $Cs_2MHy_2PbI_3Br_3$ with Br^- occupying the positions of ions acting as hydrogen-bond (HB) acceptors and I^- occupying non-interacting sites. This preferential occupation leads to a giant increase of the octahedral distortion (27- and 249-fold, compared to the bromide and iodide, respectively). Raman spectra confirm the static disorder of MHy^+ and preferential occupation of halide sites. With the use of linear optical measurements, we demonstrate that all compounds exhibit broadband orange-yellow emission attributed to self-trapped excitons (STEs). The observed Stokes shifts of $Cs_2MHy_2PbBr_6$ and $Cs_2MHy_2PbBr_3I_3$ are record large among 0D lead halides. A large increase of the octahedral distortion due to the preferential occupation of halide sites in $Cs_2MHy_2PbBr_3I_3$ is reflected in the spectra by broadening and red-shift of its emission. This study paves the way for developing a new class of light-emitting 0D lead halides by synthesizing mixed-cation analogues.

Received 30th August 2023,
Accepted 20th October 2023

DOI: 10.1039/d3qi01749d

rsc.li/frontiers-inorganic

1. Introduction

Inorganic and hybrid organic–inorganic lead halides have attracted a lot of attention in recent years due to their functional properties. In this respect, three-dimensional (3D) perovskites of general formula $APbX_3$ (A = methylammonium (MA^+), formamidinium (FA^+), aziridinium (AZR^+), MHy^+, Cs^+; X = Cl^-, Br^-, I^-) are attractive solar cell, light-emitting and nonlinear optical (NLO) materials.[1–11] These 3D perovskites can be obtained for a few above-mentioned small cations only whereas for other organic cations two-dimensional (2D), one-dimensional (1D) and discrete (0D) structures can be prepared. Lowering of dimensionality leads to widening of the bandgap and increase of the exciton binding energy, limiting their photovoltaic performance.[12–14] Low-dimensional lead halides are, however, attractive materials for NLO,[15,16] dielectric switching,[17] ferroelectric[16,18] and light-emitting applications.[13,14,19,20] It is worth adding that low dimensional structures can also be obtained using a mixed cation approach. The most famous families of compounds containing two cations are the alternating cations in the interlayer (ACI, $(B)A_nPb_nX_{3n+1}$) perovskites as well as multilayered ($n \geq 2$) Dion–Jacobson (DJ, $A''A_{n-1}Pb_nX_{3n+1}$) and Ruddlesden–Popper (RP, $A'_2A_{n-1}Pb_nX_{3n+1}$) compounds (A′ and A″ are large monovalent and divalent cations, respectively; B is a small or large monovalent cation; n indicates the number of octahedral layers within each inorganic slab).[12,15,18,19,21] The two-cation approach in these layered perovskites allows the narrowing of the bandgap, which is beneficial for solar cell applications.[12] This approach is also an efficient way for tuning photoluminescence (PL) colour as well as inducing polar (ferro- or antiferroelectric) order and second-order NLO properties.[15,18,19,21,22] Although numerous examples of layered lead halide perovskites comprising two cations have been reported, we are not aware of any mixed-cation analogues in the family of 1D and 0D lead halides.

The PL of 3D and non-corrugated 2D lead halides usually consists of narrow bands attributed to free exciton (FE) recombination.[10,11,13,14,16,19] Unfortunately, this narrow emis-

W. Trzebiatowski Institute of Low Temperature and Structural Research of the Polish Academy of Sciences, Okólna 2, 50-422 Wroclaw, Poland.
E-mail: M.Maczka@intibs.pl

†Electronic supplementary information (ESI) available: Tables S1–S6: details of structural parameters, Raman wavenumbers together with the proposed assignment and comparison of optical parameters for 0D lead halides. Fig. S1–S11: powder X-ray diffractograms, temperature evolution of lattice parameters for $Cs_2MHy_2PbBr_6$, Raman spectra, PL excitation spectra, decay curves and the logarithm of $I_0/I - 1$ as a function of $1/kT$ plots for $Cs_2MHy_2PbX_6$ compounds. CCDC 2269853–2269855. For ESI and crystallographic data in CIF or other electronic format see DOI: https://doi.org/10.1039/d3qi01749d

sion has a relatively low PL quantum yield (PLQY). Lowering the dimensionality to 1D and 0D promotes self-trapping of excitons, leading to the appearance of heavily Stokes shifted broadband PL from STEs with high PLQYs.[12–14,23] In particular, high PLQYs can be realized in 0D lead halides since due to the fact that they are composed of isolated PbX_6^{4-} octahedra or lead halide clusters, they usually have a strong exciton binding energy that increases radiative recombination.[12–14,23] 0D perovskites are also much more stable under ambient conditions than 3D, 2D or 1D analogues, which is beneficial for applications.[13] The stability can be further increased by partially replacing organic cations with inorganic ones, as reported for the lead-free $DFPD_2CsBiI_6$ compound (DFPD = 4,4-difluoropiperidine).[24]

Although 0D metal halides have received much attention in recent years, the number of discovered 0D lead halides is still scarce. The most famous are all-inorganic Cs_4PbX_6 compounds, composed of isolated PbX_6 octahedra surrounded by Cs^+ ions.[13,23,25–27] PL was reported for Cs_4PbBr_6 but it consisted of a relatively narrow green emission.[13,23,25–27] Therefore, its mechanism is still controversial and some reports attributed it to $CsPbBr_3$ impurities, inclusion-induced emission or defect state-induced emission.[23] Recent studies supported the assignment of the green emission to the presence of luminescent $CsPbBr_3$ inclusions.[27] Among iodides and chlorides, the known examples are $MA_4PbI_6{\cdot}2H_2O$, which consists of isolated octahedral units,[28] $(C_9NH_{20})_7(PbCl_4)Pb_3Cl_{11}$, which consists of $PbCl_4^{2-}$ tetrahedra and $Pb_3Cl_{11}^{5-}$ trimer clusters,[29] and $(TAE)_2[Pb_2Cl_{10}]Cl_2$ (TAE = tris(2-aminoethyl) ammonium), containing isolated lead chloride edge sharing bioctahedra $Pb_2Cl_{10}^{6-}$.[30] $(C_9NH_{20})_7(PbCl_4)Pb_3Cl_{11}$ exhibited blue emission near 470 nm with a very high PLQY (near 83%),[29] whereas $(TAE)_2[Pb_2Cl_{10}]Cl_2$ showed white emission.[30] There are also several bromides composed of isolated $PbBr_6^{4-}$ octahedra,[31] isolated $PbBr_4^{2-}$ units,[32,33] and lead–bromide clusters,[34–36] which exhibit broadband emissions.

In this paper, we report a new approach to developing 0D lead halides by employing both organic (MHy^+) and inorganic (Cs^+) cations. We investigate the crystal structures and optical properties of the obtained 0D mixed organic–inorganic lead halides.

2. Experimental section

2.1. Synthesis

In order to obtain single crystals of $Cs_2MHy_2PbBr_6$, 1 mmol $PbBr_2$ (98%, Sigma Aldrich) was dissolved in 8 mL of HBr (48 wt% in H_2O, Sigma-Aldrich). Then 2 mmol Cs_2CO_3 and 1 mL of methylhydrazine (98%, Sigma Aldrich) were added under vigorous stirring. The solution was heated to 50 °C and then 10 mL of propylene carbonate (PC, 99.7%, Sigma-Aldrich) was added. The reaction mixture was cooled down to room temperature (RT) and left undisturbed. Colourless transparent crystals, which grew at the bottom of the glass vial, were separated from the mother liquid, washed 3 times with ethanol and dried at RT. Colourless $Cs_2MHy_2PbBr_3I_3$ and light yellow $Cs_2MHy_2PbI_6$ crystals were grown using the same procedure but with smaller amounts of PC, *i.e.*, 7 and 5 mL, respectively. PbI_2 (99%, Sigma Aldrich) and HI (57 wt% in H_2O, stabilized with H_3PO_2) were purchased from Sigma-Aldrich.

We also grew single crystals of inorganic $CsPbBr_3$ and Cs_4PbBr_6. In order to grow single crystals of $CsPbBr_3$, 5 mmol CsBr (99.9%, Sigma-Aldrich) and 6 mmol $PbBr_2$ were dissolved in 10 mL of dimethyl sulfoxide (DMSO, 99.9%, Sigma-Aldrich) under stirring for 24 h at RT. The reaction mixture was then left at 40 °C and the orange crystals, which grew in the vial after 4 days, were separated from the mother liquid, washed with ethanol and dried at RT. Yellow crystals of Cs_4PbBr_6 were prepared in the same procedure but the reaction mixture contained 2 mmol of $PbBr_2$ and 10 mmol of CsBr.

The powder X-ray diffraction patterns of the obtained crystals are in good agreement with the calculated ones based on single-crystal diffraction data (Fig. S1, ESI†), confirming the purity of the bulk sample.

2.2. Powder X-ray diffraction

Powder X-ray diffraction (PXRD) patterns of the ground crystals were measured in the reflection modes using an X'Pert PRO X-ray diffraction system equipped with a PIXcel ultrafast line detector and Soller slits for CuKα_1 radiation (λ = 1.54056 Å).

2.3. Single-crystal X-ray diffraction

The single-crystal X-ray diffraction experiments were conducted using a conventional Xcalibur four-circle diffractometer from Oxford Diffraction. The experiments utilized Mo $K_{\alpha1\alpha2}$ radiation and a CCD (Atlas) camera. The empirical absorption correction using spherical harmonics was done in the SCALE3 ABSPACK scaling algorithm implemented in CrysAlis PRO 1.171.39.46 (Rigaku Oxford Diffraction, 2018). For solving and refining the structures, the ShelxT and ShelXL were employed, respectively.[37,38] Hydrogen atoms were introduced at calculated positions and refined as riding atoms. The measurements were conducted both at RT (295 K) and 100 K, and no symmetry changes were observed, confirming the temperature stability of new materials. The details on the measured samples and refinement are shown in ESI, Table S1.† Pb–X distances are given in Table S2,† whereas Table S3† shows the geometry of possible hydrogen-bond interactions. Fig. S2† presents the temperature evolution of lattice parameters and unit cell volume in $Cs_2MHy_2PbBr_6$, which confirms the stability of the RT structure at low-temperatures. The refinements show the regions of negative electron density with the highest of −2.54 e A^{-3} at 0.65 Å from Cs^+ in $Cs_2MHy_2PbI_6$, which may denote the presence of MHy^+ also at Cs^+ sites. CCDC deposition numbers: 2269853–2269855.†

2.4. Raman spectroscopy

The RT Raman spectra of powdered crystals in the 3500–100 cm^{-1} range were recorded using a Bruker FT 100/S spectrometer with YAG:Nd laser excitation (λ_{exc} = 1064 nm) and 2 cm^{-1} spectral resolution. Additional low-wavenumber

Raman spectra in the 500–10 cm^{-1} range were measured using a Renishaw inVia Raman spectrometer (Renishaw, UK), equipped with a confocal DM2500 Leica optical microscope, a thermoelectrically cooled CCD as a detector, an eclipse filter and a diode laser operating at 830 nm.

2.5. Optical absorption and photoluminescence (PL) studies

The RT diffuse reflectance spectra of the powdered samples were recorded using a Varian Cary 5E UV–Vis–NIR spectrophotometer (Varian, Palo Alto, CA, USA). Temperature-dependent emission spectra were recorded under 266 nm excitation from a laser diode and with a Hamamatsu PMA-12 photonic multichannel analyser, equipped with a BT-CCD linear image sensor (Hamamatsu Photonics, Iwata, Japan). The temperature of the samples was controlled using a Linkam THMS 600 heating/freezing stage (Linkam, Tadworth, UK). To record decay times, a femtosecond laser (Coherent Model Libra) (Coherent, Pennsylvania, USA) was used as an excitation source.

3. Results and discussion

3.1 Single-crystal X-ray diffraction

The crystal structure of ternary lead halides of the Cs_4PbX_6 formula, where X = Cl, Br, or I was initially reported by C. K. N. Moller,[39] and subsequently confirmed by R. H. Andrews *et al.*[40] and K. Nitsch *et al.*[41] These compounds exhibit a rhombohedral crystal structure belonging to the $R\bar{3}c$ space group (no. 167). The Pb and halogen atoms form slightly distorted PbX_6^{4-} octahedra, which are isolated (0D). Notably, the Pb–X distances in Cs_4PbX_6 are longer compared to those observed in the 3D $CsPbX_3$ structures. Recent synchrotron and X-ray diffraction experiments, along with Raman and PL spectroscopy conducted on Cs_4PbBr_6, confirmed the rhombohedral packing under normal conditions.[27] These experiments also revealed high-pressure phase transition occurring at P = 2.9 GPa to an orthorhombic crystal structure belonging to the *Cmce* space group. This orthorhombic phase remains stable within the pressure range of 2.9 to 4.2 GPa. Above the triclinic symmetry is thermodynamically favoured. It is worth noting that octahedral coordination is only slightly disturbed by I to II high-pressure phase transition.

$Cs_2MHy_2PbX_6$ compounds, where X = Br and I, adopt crystal structures analogous to ternary Cs_4PbX_6. However, the symmetry of these hybrid crystals is related to the high-pressure modification of Cs_4PbBr_6. The presence of larger and highly anisotropic counterions in the crystal structure creates internal pressure on the inorganic component, leading to the octahedral distortions of *Cmce* symmetry. Until now, there have been no reports on the discrete 0D structures of MHy-based metal-halide hybrids.

The crystal packing of $Cs_2MHy_2PbX_6$ is shown in Fig. 1. The characteristic feature is the layered arrangement of the structure components. The MHy^+ selectively substitute for Cs^+ ions forming hydrogen bonded (HB) layers interacting *via* N–H···X bonds with the inorganic part. In $Cs_2MHy_2PbBr_6$ the presence of the organic component significantly changes the a and c unit cell parameters, which expands from a = 13.2887(20) Å, b = 12.6058(20) Å, and c = 9.5105(20) Å in all-inorganic Cs_4PbBr_6,[27] to a = 14.280(4) Å, b = 12.876(4) Å, and c = 10.772(4) Å in the hybrid.

The inherent property of the crystal structure of $Cs_2MHy_2PbX_6$ is the disorder of MHy^+ cations. It is present both at 295 K and 100 K, has statistical character and results in two equivalent positions of MHy^+ related by the mirror m plane, which makes terminal CH_3 and NH_2 groups undistinguishable. The selective substitution of halide ions in $Cs_2MHy_2PbI_3Br_3$ mixed crystals is also worth noting where the positions of ions acting as HB acceptors are preferentially occupied by Br^-. The best refinement results were obtained for the model with full occupancy of Br^- at interacting sites, and mixed occupancy of non-interacting sites with 0.75 and 0.25 of I and Br, respectively. The Pb–Br bond lengths also seem to positively verify this model, as in $Cs_2MHy_2PbBr_6$ as well as in the mixed-halide $Cs_2MHy_2PbI_3Br_3$ the Pb–Br distances to Br^- interacting with MHy^+ are roughly the same (3.011 *vs.* 3.037 Å). Additionally, this preferential substitution leads to a significantly larger octahedral distortion parameter in mixed crystals as it grows from 0.12×10^{-5} and 1.1×10^{-5} in $PbBr_6^{4-}$ and PbI_6^{4-}, respectively, to 29.9×10^{-5} in $[PbBr_3I_3]^{4-}$. Fig. 2 shows the HB layers, disordered MHy^+ positions and illustrates the preferential location of halogen Br^- and I^- ions in mixed $Cs_2MHy_2PbI_3Br_3$.

3.2. Raman study

Raman spectra of $Cs_2MHy_2PbX_6$ and Cs_4PbBr_6 samples are shown in Fig. 3 and S3, S4,† and the observed modes are listed in Tables S4 and S5† together with the assignment based on previous studies of MHy-based 3D, 2D and 1D lead halide perovskites and all-inorganic Cs_4PbBr_6.[6,27,42–45] Fig. 3 and S3, and Table S4† show that bands related to vibrations of the CH_3 groups are observed at very similar wavenumbers as previously reported for 3D, 2D and 1D analogues whereas bands related to vibrations of the NH_2 and NH_2^+ groups are much more sen-

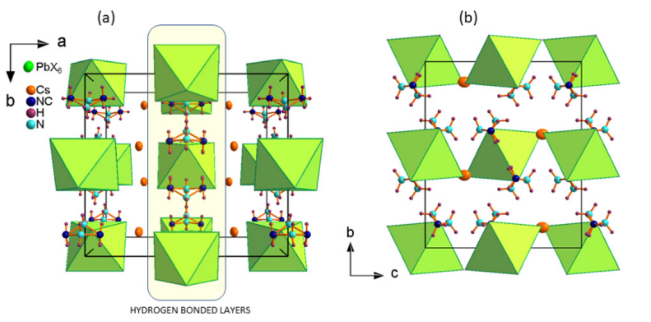

Fig. 1 The crystal structures of $Cs_2MHy_2PbX_6$ and MHy^+ are disordered. (a) Discrete (0D) Pb $(Br/I)_6$ units interact through HBs with MHy^+ cations forming HB layers perpendicular to the *a* direction, coulombic interactions between caesium ions and $Pb(Br/I)_6$ units stabilize the structure perpendicular to the layers. (b) The view along the *a* direction.

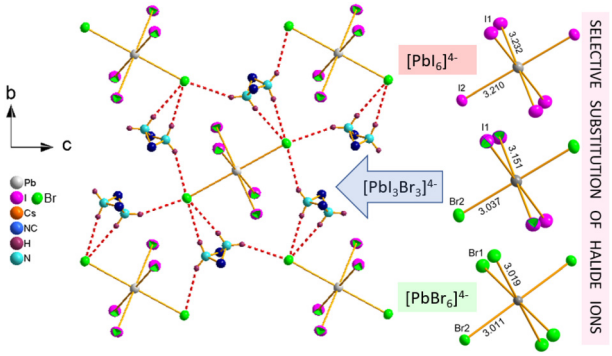

Fig. 2 The N–H···Br HB network in $Cs_2MHy_2Pb(Br/I)_6$. In each $Pb(Br/I)_6$ there are two sites for halogen ions interacting with middle-chain NH_2^+ groups. In $Cs_2MHy_2PbI_3Br_3$ they are preferentially occupied by Br^-.

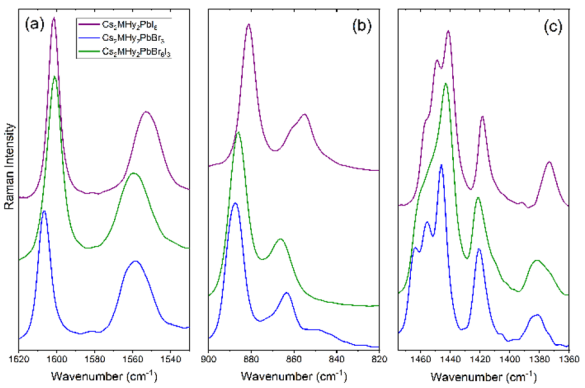

Fig. 3 Raman spectra of $Cs_2MHy_2PbX_6$ compounds in the (a) 1620–1530 cm^{-1}, (b) 900–820 cm^{-1} and (c) 1475–1360 cm^{-1} wavenumber range showing behaviour of NH_2^+-related modes (bands near 1560, 860 and 1360 cm^{-1}), the NH_2-related mode (band near 1600 cm^{-1}), CH_3-related modes (bands in the 1463–1418 cm^{-1} range) and the ν_s(CNN) mode near 890 cm^{-1}.

sitive on the crystal structure. For instance, the $\nu_s(NH_2)$ mode of the terminal NH_2 group exhibits shift to a lower wavenumber when going from 2D MHy_2PbBr_4 (3247 cm^{-1}) to 0D $Cs_2MHy_2PbBr_6$ (3236 cm^{-1}), 1D $MHyPbI_3$ (3217 cm^{-1}) and 3D $MHyPbBr_3$ (3217 cm^{-1}) (Table S4†). This shift indicates that the strength of the HB between the halogen anion and the NH_2 group increases in the order 2D < 0D < 1D < 3D. In general, the strong sensitivity of the NH_2 and NH_2^+ modes on the type of crystal structure points to significantly different HB networks in these compounds.

Former temperature-dependent studies of MHy-based perovskites showed that the disorder of MHy^+ cations is reflected in the spectra by broadening of Raman bands, especially pronounced for those related to the NH_2^+ and NH_2 groups.[6,42,43,46,47] These bands are narrow for $Cs_2MHy_2PbX_6$ analogues, *i.e.*, their widths are comparable to Raman widths of well-ordered $MHyPbBr_3$ and $MHyPbI_3$. For instance, the full width at half maximum (FWHM) of the $\rho(NH_2^+)$ mode is about 11.3 cm^{-1} for $Cs_2MHy_2PbBr6_6$, 10.6 cm^{-1} for $MHyPbBr_3$ and 7.5 cm^{-1} for $MHyPbI_3$. Narrow Raman bands confirm that the disorder revealed by X-ray diffraction is not dynamic but static.

Raman spectra of $Cs_2MHy_2PbX_6$ compounds in the internal mode region are very similar (Fig. 3 and S3†), confirming the same crystal structure. Replacement of Br^- by I^- leads to a weak shift of Raman bands to lower wavenumbers (Table S4†) due to a larger size of the latter anion. In case of the mixed halide compound, $Cs_2MHy_2PbBr_3I_3$, a clear shift to lower wavenumbers compared to $Cs_2MHy_2PbBr_6$ is observed for bands related to vibrations of the CH_3 and terminal NH_2 groups (Table S4, Fig. S3† and Fig. 3). Positions of bands related to the middle NH_2^+ groups are, however, close to those observed for pure bromide (Table S4,† Fig. 3 and S3†). Raman spectra confirm, therefore, the X-ray diffraction model with preferential occupation by Br^- at the sites interacting *via* HBs with the NH_2^+ groups. Closer inspection of the Raman spectra also shows that some bands become broader and less resolved for the mixed-halide compound. This behaviour, observed for instance for the $\delta_{as}(CH_3)$ bands in the 1463–1441 cm^{-1} (Fig. 3c), reflects compositional disorder at sites occupied by both Br^- and I^-.

A comparison of low-wavenumber Raman spectra shows that the majority of modes exhibit large shifts to lower wavenumbers when Br^- is replaced by I^-. This behaviour is related to a larger size and atomic mass of I^- compared to Br^-. Raman modes of all-inorganic Cs_4PbBr_6 show weak shifts to higher wavenumbers when compared to $Cs_2MHy_2PbBr_6$. This effect can be attributed to the smaller unit-cell size of the former compound. It is worth noting that the bands of Cs_4PbBr_6 are narrower than the corresponding bands of $Cs_2MHy_2PbBr_6$. This behaviour is consistent with more pronounced dynamics of MHy^+ compared to Cs^+.

3.3. Optical properties

The RT diffuse absorption spectra of the investigated samples consist of two bands positioned in the UV region (Fig. 4). The lower energy and less intense band is observed at 332 nm (3.73 eV), 372 nm (3.33 eV) and 395 nm (3.14 eV) for $Cs_2MHy_2PbBr_6$, $Cs_2MHy_2PbBr_3I_3$, and $Cs_2MHy_2PbI_6$, respectively. The second higher energy and more intense band appeared at 305 nm (4.07 eV), 331 nm (3.75 eV) and 357 nm (3.47 eV) for $Cs_2MHy_2PbBr_6$, $Cs_2MHy_2PbBr_3I_3$, and $Cs_2MHy_2PbI_6$, respectively. This band is broadened for the mixed-halide $Cs_2MHy_2PbBr_3I_3$. The spectrum of all-inorganic Cs_4PbBr_6 also shows two bands at 329 nm (3.77 eV) and 307 nm (4.04 eV), *i.e.*, this spectrum is very similar to the spectrum of $Cs_2MHy_2PbBr_6$. Very similar two bands were previously reported by other authors for samples prepared from single crystals by grinding,[48,49] but studies of nanocrystalline and thin films usually showed the presence of only one band at 284 nm (4.37 eV) for Cs_4PbCl_6, 310–314 nm (3.95–3.99 eV) for Cs_4PbBr_6, and 365–367 nm (3.38–3.4 eV) for Cs_4PbI_6.[26,50,51] Based on literature data and DFT calculations performed for Cs_4PbBr_6,[48,50] the observed absorption bands can be attributed to the localized absorption from the isolated PbX_6 octahedra. DFT calculations proved that the localized density of states (DOS) corresponding to these bands is mainly composed of Br-

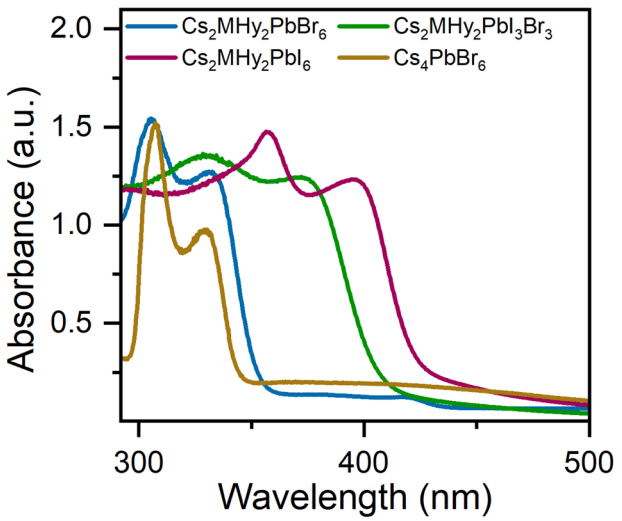

Fig. 4 The 300 K diffuse absorption spectra of the investigated perovskites.

4p and Pb-6s orbitals whereas Cs orbitals almost have no contribution to the DOS near the valence band and conduction band.[48,50] In general, the absorption bands of 0D halides are observed in narrow ranges, *i.e.*, 367–395 nm (3.14–3.47 eV), 305–348 nm (3.56–4.07 eV) and 284–348 nm (3.56–4.37 eV) for the iodides, bromides and chlorides, respectively (Table S6†).

The PL excitation (PLE) and emission (PL) spectra of the synthesized hybrid crystals recorded at 80 K are shown in Fig. 5a. As can be seen, PL spectra consist of one broad band centred at 637 nm and 647 nm with FWHM values of 158 and 175 nm for $Cs_2MHy_2PbI_6$ and $Cs_2MHy_2PbBr_6$, respectively (Table S6†). The emission of the mixed-halide compound is much broader with an FWHM of 230 nm and is red-shifted to 680 nm. This behaviour can be attributed to significantly larger octahedral distortion in $Cs_2MHy_2PbBr_3I_3$, as revealed by the X-ray diffraction study. The large Stokes shift and broad emission are characteristic of STE emission.[52,53] The excitation spectra monitored at the maximum of the emission contain three bands located in the 300–450 nm spectral range and indicate the presence of additional states below the bottom of the conduction band (Fig. 5a). The emission-wavelength-dependent PL excitation spectra of the representative $Cs_2MHy_2PbBr_6$ sample exhibit various profiles at different

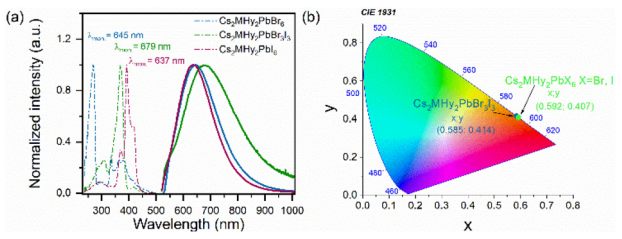

Fig. 5 (a) Low temperature (80 K) PLE (dashed) and PL spectra (solid) and (b) CIE coordinates of $Cs_2MHy_2PbX_6$ (X = Br, I) and $Cs_2MHy_2Br_3I_3$ crystals.

monitored wavelengths (Fig. S5†). This confirms the presence of more than one PL centre, which could be assigned to STE emission. Similar broadband and strongly Stokes shifted emissions have been reported for many low-dimensional lead halide perovskites,[19,20,44,52,54–56] including 0D.[29–36,53,57] Table S6† shows that $Cs_2MHy_2PbBr_6$ and $Cs_2MHy_2PbBr_3I_3$ exhibit a record large Stokes shift among 0D lead halides.

To confirm the origin of the PL bands, we have also performed time-resolved measurements at 80 K under a 266 nm excitation line generated with a femtosecond laser. It can be seen that the registered decay curves were non-exponential with faster (around 0.33 μs) and longer components. The longest lifetime of 1.16 μs is observed for the Br-analogue and it decreases to 0.87 μs and 0.79 μs for $Cs_2MHy_2PbBr_3I_3$ and $Cs_2MHy_2PbI_6$, respectively (Fig. S6†). A longer lifetime of 7.79 μs is observed for all-inorganic Cs_4PbBr_6 (Fig. S7†). The obtained lifetimes are much longer than the values reported for the HOMO–LUMO electronic transitions of the organic cation, proving that the observed emission comes from trapped states.[6,46] Similarly long lifetimes of 5.8 and 16.4 μs were, however, reported for 0D *N*-benzylpyridinium$_6Pb_3Br_{12}$ and $(C_{13}H_{19}N_4)_2PbBr_4$.[33,34]

It is worth noting that in spite of very similar crystal structures of $Cs_2MHy_2PbBr_6$ and all-inorganic Cs_4PbBr_6, the latter compound shows significantly different emissions. As can be seen in Fig. S8,† the PL of Cs_4PbBr_6 is narrow (FWHM = 9 nm) and centred at 531 nm. Furthermore, the band at 531 nm corresponds well to the 530 nm band of $CsPbBr_3$. Our results are, therefore, consistent with the assignment of Cs_4PbBr_6 PL to $CsPbBr_3$ inclusions and lack of efficient emission from the Cs_4PbBr_6 matrix.[27] They also show that partial replacement of Cs^+ by organic cations (*e.g.*, MHy^+) is an effective way to induce efficient broadband PL in these perovskites. Based on the PL spectra, the CIE coordinates of $Cs_2MHy_2PbX_6$ (X = Br, I) and $Cs_2MHy_2PbBr_3I_3$ crystals were calculated and are shown in Fig. 5b. The calculated values are characteristic of the orange-yellow emission.

The emission intensity of all investigated lead halides strongly depends on temperature (Fig. 6). The position and shape of the emission bands do not change upon heating. However, the emission intensity significantly decreases with an increase in temperature with $T_{0.5}$ = 105 K. To estimate the activation energies of thermal quenching, the Arrhenius equation was used (Fig. S9–S11†):

$$I(T) = \frac{I_0}{1 + c \cdot \exp\left(\frac{-E_a}{k_b T}\right)} \quad (1)$$

where I_0 is the initial intensity of luminescence (80 K), $I(T)$ is the intensity at a given temperature T, c is a constant value, E_a is the activation energy of thermal quenching, and k is Boltzmann's constant. The emission of $Cs_2MHy_2PbBr_3I_3$ is less stable with an E_a value of 51 meV, while the emissions of the iodide and bromide analogues are more stable with E_a values of 57 meV and 65 meV, respectively. These values are similar

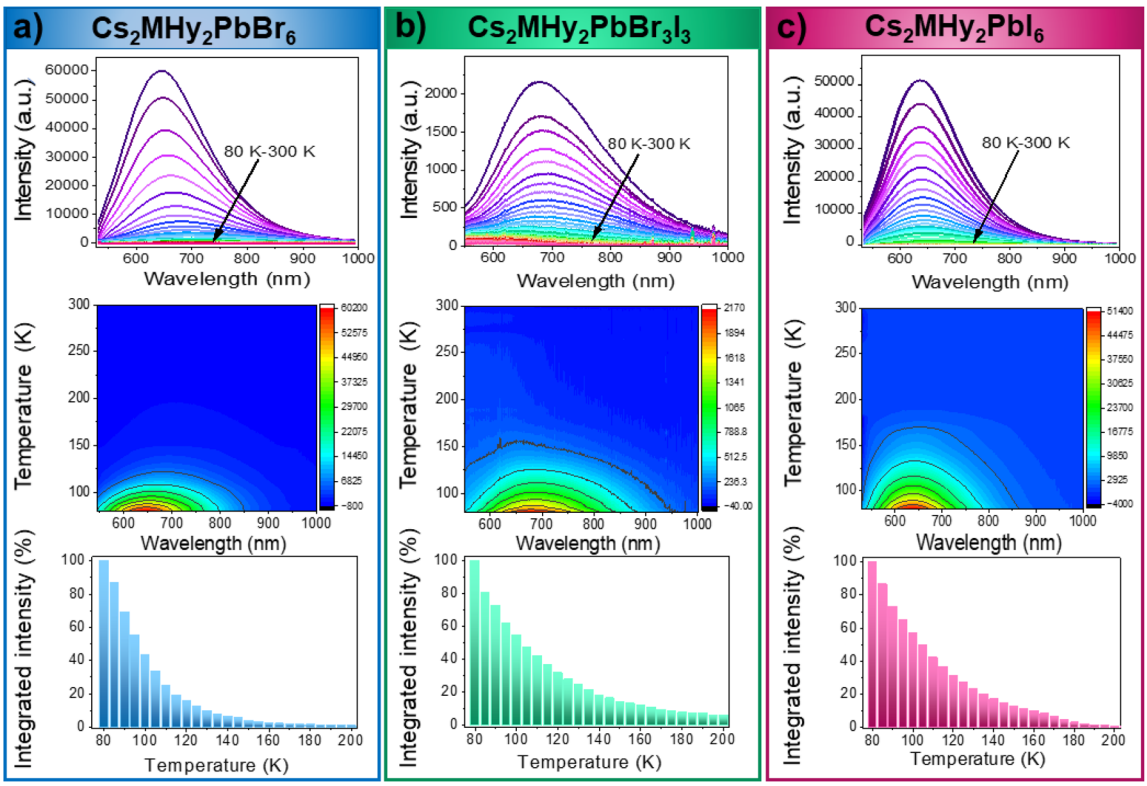

Fig. 6 Temperature-dependent emission spectra recorded from 80 to 300 K, the PL intensity contour map, and the integrated emission intensity at various temperatures of (a) $Cs_2MHy_2PbBr_6$, (b) $Cs_2MHy_2PbBr_3I_3$, and (c) $Cs_2MHy_2PbI_6$, respectively.

to that reported for 3D $MHyPbBr_3$ (63 meV),[6] smaller than that of 2D MHy_2PbBr_4 (99.9 meV)[16] and significantly larger than that of 0D $(TAE)_2[Pb_2Cl_{10}]Cl_2$ (5 meV).[30]

4. Conclusions

For the first time, a mixed-cation approach has been successfully employed to synthesize three newcomers to the small family of 0D lead halides. The obtained $Cs_2MHy_2PbBr_6$, $Cs_2MHy_2PbBr_3I_3$, and $Cs_2MHy_2PbI_6$ isostructural compounds crystallize in orthorhombic structures (space group *Cmce*). The structures are built up of isolated PbX_6^{4-} octahedral units. The characteristic feature of these structures, not reported for other MHy-based perovskites, is the static disorder of MHy^+ cations, which form HBs with halide anions. X-ray diffraction also reveals that in the mixed halide analogue, $Cs_2MHy_2PbI_3Br_3$, Br^- (I^-) anions preferentially occupy the sites acting (non-acting) as HB acceptors. This preferential substitution leads to a significantly larger octahedral distortion parameter in $Cs_2MHy_2PbBr_3I_3$ crystals.

Raman studies show that the HB strength in the discovered 0D lead halides is stronger than in 2D MHy_2PbBr_4 but weaker than in 1D $MHyPbI_3$ and 3D $MHyPbBr_3$. Raman data also confirm the preferential occupation of anionic sites by Br^- and I^- in the mixed-halide analogue as well as the static character of MHy^+ disorder in all compounds.

Linear optical studies demonstrate that $Cs_2MHy_2PbBr_6$ and $Cs_2MHy_2PbI_6$ exhibit broadband orange-yellow PL with maxima (FWHM) at 637 (158) and 647 nm (175 nm), respectively, and vast Stokes shifts of 342 and 280 nm for $Cs_2MHy_2PbBr_6$ and $Cs_2MHy_2PbI_6$, respectively. To the best of our knowledge, $Cs_2MHy_2PbI_6$ is the first 0D iodide for which PL was reported. Much larger octahedral distortion in mixed-cation $Cs_2MHy_2PbBr_3I_3$ manifests a red-shift of PL to 680 nm and an increase of FWHM to 230 nm. For this compound, the Stokes shift is 349 nm. The observed Stokes shifts for $Cs_2MHy_2PbBr_6$ and $Cs_2MHy_2PbBr_3I_3$ are record large among the family of 0D lead halides. The PL of $Cs_2MHy_2PbX_6$ compounds shows strong temperature dependence and analysis of these data reveals that the activation energies required for thermal quenching are 51, 57 and 65 meV for $Cs_2MHy_2PbBr_3I_3$, $Cs_2MHy_2PbI_6$ and $Cs_2MHy_2PbBr_6$, respectively.

Overall, our results demonstrate that the mixed-cation approach is a promising way to develop novel 0D lead halides with efficient broadband PL. They also show that MHy^+ cations have unusual ability to form lead halides of vast structural diversity and properties, *i.e.*, 3D ($MhyPbX_3$, X = Cl, Br)[6–8] and quasi-2D RP ($BA_2MHy_2Pb_3Br_{10}$, BA^+ = butylammonium)[58] with MHy^+ serving as a 'perovskitizer' cation, 2D of formula MHy_2PbX_4 (X = Cl, Br, I)[16,46,47] and the 2D ACI phase ($IMMHyPbX_4$, X = Cl, Br, IM = imidazolium)[22] with MHy^+ as a 'spacer' cation and 1D ($MHyPbI_3$)[45] and 0D (this work), in

which MHy^+ cations separate inorganic chains or PbX_6^{4-} octahedra.

Author contributions

Conceptualization: M. M. Data curation: D. D., D. S. and A. G. Formal analysis: D. D., D. S. and A. G. Funding acquisition: M. M. Investigation: D. D., D. S. and A. G. Methodology: all authors. Project administration: M. M. Resources: M. M. Supervision: M. M. Validation: D. D., D. S. and A. G. Writing – original draft: all authors. Writing – review and editing: all authors. All the authors have given their approval to the final version of the manuscript.

Conflicts of interest

There are no conflicts to declare.

Acknowledgements

This research was supported by the National Science Center (Narodowe Centrum Nauki) in Poland under project no. 2019/35/B/ST5/00043.

References

1 Y. Tu, J. Wu, G. Xu, X. Yang, R. Cai, Q. Gong, R. Zhu and W. Huang, Perovskite Solar Cells for Space Applications: Progress and Challenges, *Adv. Mater.*, 2021, **33**, 2006545.
2 T. Yang, L. Gao, J. Lu, C. Ma, Y. Du, P. Wang, Z. Ding, S. Wang, P. Xu, D. Liu, *et al.*, One-Stone-for-Two-Birds Strategy to Attain Beyond 25% Perovskite Solar Cells, *Nat. Commun.*, 2023, **14**, 839.
3 Y. Zhou, Y. Huang, Z. Fan, J. B. Khurgin and Q. Xiong, Nonlinear Optical Properties of Halide Perovskites and Their Applications, *Appl. Phys. Rev.*, 2020, 041313.
4 H. Liu, H. Zhang, H. Xu and L. Zhang, The Opto-Electronic Functional Devices Based on Three-Dimensional Lead Halide Perovskite, *Appl. Sci.*, 2021, **11**, 1453.
5 W. Chen, S. Bhaumik, S. A. Veldhuis, G. Xing, Q. Xu, M. Grätzel, S. Mhaisalkar, N. Mathews and T. C. Sum, Giant Five-Photon Absorption from Multidimensional Core-shell Halide Perovskite Colloidal Nanocrystals, *Nat. Commun.*, 2017, **8**, 15198.
6 M. Mączka, M. Ptak, A. Gągor, D. Stefańska, J. K. Zaręba and A. Sieradzki, Methylhydrazinium Lead Bromide: Noncentrosymmetric Three-Dimensional Perovskite with Exceptionally Large Framework Distortion and Green Photoluminescence, *Chem. Mater.*, 2020, **32**, 1667–1673.
7 M. Mączka, A. Gągor, J. K. Zaręba, D. Stefańska, M. Drozd, S. Balciunas, M. Simenas, J. Banys and A. Sieradzki, Three-Dimensional Perovskite Methylhydrazinium Lead Chloride with Two Polar Phases and Unusual Second-Harmonic Generation Bistability above Room Temperature, *Chem. Mater.*, 2020, **32**, 4072–4082.
8 D. Drozdowski, A. Gągor, D. Stefańska, J. K. Zaręba, K. Fedoruk, M. Mączka and A. Sieradzki, Three-Dimensional Methylhydrazinium Lead Halide Perovskites: Structural Changes and Effects on Dielectric, Linear, and Nonlinear Optical Properties Entailed by the Halide Tuning, *J. Phys. Chem. C*, 2022, **126**, 1600–1610.
9 H. R. Petrosova, O. I. Kucheriv, S. Shova and I. A. Gural'skiy, Aziridinium Cation Templating 3D Lead Halide Hybrid Perovskites, *Chem. Commun.*, 2022, **58**, 5745–5748.
10 D. Stefańska, M. Ptak and M. Mączka, Photoluminescence and Vibrational Properties of Aziridinium Lead Halide Perovskites, *Molecules*, 2022, **27**, 7949.
11 O. A. Semenikhin, O. I. Kucheriv, L. Sacarescu, S. Shova and I. A. Gural'skiy, Aziridinium Cation Templating 3D Lead Halide Hybrid Perovskites, *Chem. Commun.*, 2023, **59**, 3566–3569.
12 T. Niu, Q. Xue and H. L. Yip, Advances in Dion-Jacobson Phase Two-Dimensional Metal Halide Perovskite Solar Cells, *Nanophotonics*, 2021, **10**, 2069–2102.
13 S. Sun, M. Lu, X. Gao, Z. Shi, X. Bai, W. W. Yu and Y. Zhang, 0D Perovskites: Unique Properties, Synthesis, and Their Applications, *Adv. Sci.*, 2021, **8**, 2102689.
14 Y. Han, S. Yue and B. B. Cui, Low-Dimensional Metal Halide Perovskite Crystal Materials: Structure Strategies and Luminescence Applications, *Adv. Sci.*, 2021, **8**, 2004805.
15 X. Han, Y. Zheng, S. Chai, S. Chen and J. Xu, 2D Organic-Inorganic Hybrid Perovskite Materials for Nonlinear Optics, *Nanophotonics*, 2020, **9**, 1787–1810.
16 M. Mączka, J. K. Zaręba, A. Gągor, D. Stefańska, M. Ptak, K. Rolder, D. Kajewski, A. Soszyński, K. Fedoruk and A. Sieradzki, $[Methylhydrazinium]_2PbBr_4$, a Ferroelectric Hybrid Organic-Inorganic Perovskite with Multiple Nonlinear Optical Outputs, *Chem. Mater.*, 2021, **33**, 2331–2342.
17 M. M. Lun, F. L. Zhou, D. W. Fu and Q. Ye, Multi-functional Hybrid Perovskites with Triple-Channel Switches and Optical Properties, *J. Mater. Chem. C*, 2022, **10**, 11371–11378.
18 P. Siwach, P. Sikarwar, J. S. Halpati and A. K. Chandiran, Design of Above-Room-Temperature Ferroelectric Two-Dimensional Layered Halide Perovskites, *J. Mater. Chem. A*, 2022, **10**, 8719–8738.
19 M. D. Smith, B. A. Connor and H. I. Karunadasa, Tuning the Luminescence of layered Halide Perovskites, *Chem. Rev.*, 2019, **119**, 3104–3139.
20 S. Smółka, M. Mączka, D. Drozdowski, D. Stefańska, A. Gągor, A. Sieradzki, J. K. Zaręba and M. Ptak, Effect of Dimensionality on Photoluminescence and Dielectric Properties of Imidazolium Lead Bromides, *Inorg. Chem.*, 2022, **61**, 15225–15238.
21 S. Shao, X. Cui and Z. Li, Recent Progress in Understanding the Structural, Optoelectronic, and Photophysical Properties of Lead Based Dion-Jacobson Perovskites as Well

as Their Application in Solar Cells, *ACS Mater. Lett.*, 2022, **4**, 891–917.

22 D. Drozdowski, K. Fedoruk, A. Kabanski, M. Maczka, A. Sieradzki and A. Gagor, Broadband Yellow And White Emission from Large Octahedral Tilting in (110)-Oriented Layered Perovskites: Imidazolium-Methylhydrazinium Lead Halides, *J. Mater. Chem. C*, 2023, **11**, 4907.

23 M. Li and Z. Xia, Recent Progress of Zero-Dimensional Luminescence Metal Halides, *Chem. Soc. Rev.*, 2021, **50**, 2626–2662.

24 T. Bai, X. Wang, Y. He, H. Wei, Y. Su and J. Chen, Turning Self-Trapped Exciton Emission to Near-Infrared Regionin Thermochromism Zero-Dimensional Hybrid Metal Halides, *Adv. Opt. Mater.*, 2023, 2301110.

25 A. A. Akkerman, A. L. Abdelhady and L. Manna, Zero-Dimensional Cesium Lead Halides: History, Properties, and Challenges, *J. Phys. Chem. Lett.*, 2018, **9**, 2326–2337.

26 U. Thumu, M. Piotrowski, B. Owens-Baird and Y. V. Kolen'ko, Zero-Dimensional Cesium Lead Halide Perovskites: Phase Transformations, Hybrid Structures, and Applications, *J. Solid State Chem.*, 2019, **271**, 361–377.

27 W. Castro Ferreira, B. S. Araujo, M. A. P. Gomez, F. E. O. Medeiros, C. W. de Araujo Paschoal, C. B. da Silva, P. T. C. Freire, U. F. Kaneko, F. M. Ardito, N. M. Souza-Neto and A. P. Ayala, Pressure-Induced Structural and Optical Transitions in Luminescent Bulk Cs_4PbBr_6, *J. Phys. Chem. C*, 2022, **126**, 541–550.

28 B. R. Vincent, K. N. Robertson, T. Stanley Cameron and O. Knop, Alkylammonium lead iodides. Part 1. Isolated PbI_6^{4-} ions in $(CH_3NH_3)_4PbI_6{\bullet}H_2O$, *Can. J. Chem.*, 1987, **65**, 1042–1046.

29 C. Zhou, H. Lin, M. Worku, J. Neu, Y. Zhou, Y. Tian, S. Lee, P. Djurovich, T. Siegrist and B. Ma, Blue Emitting Single Crystalline Assembly of Metal Halide Clusters, *J. Am. Chem. Soc.*, 2018, **140**, 13181–13184.

30 S. Elleuch, A. Lusson, S. Pillet, K. Boukheddaden and Y. Abid, White Light Emission from a Zero-Dimensional Lead Chloride YHybrid Material, *ACS Photonics*, 2020, **7**, 1178–1197.

31 B. B. Cui, Y. Han, B. Huang, Y. Zhao, X. Wu, L. Liu, G. Cao, Q. Du, N. Liu, W. Zou, M. Sun, L. Wang, X. Liu, J. Wang, H. Zhou and Q. Chen, Locally Collective Hydrogen Bonding Isolates Lead Octahedra for White Emission Improvement, *Nat. Commun.*, 2019, **10**, 5190.

32 V. Morad, Y. Shynkarenko, S. Yakunin, A. Brumberg, R. D. Schaller and M. V. Kovalenko, Disphenoidal Zero-Dimensional Lead, Thin and Germanium Halides: Highly Emissive Singlet and Triplet Self-Trapped Excitons and X-ray Scintillation, *J. Am. Chem. Soc.*, 2019, **141**, 9764–9768.

33 H. Lin, C. Zhou, M. Chaaban, L. J. Xu, Y. Zhou, J. Neu, M. Worku, E. Berkwits, Q. He, S. Lee, X. Lin, T. Siegrists, M. H. Du and B. Ma, Bulk Assembly of Zero-Dimensional Organic Lead Bromide Hybrid with Efficient Blue Emission, *ACS Mater. Lett.*, 2019, **1**, 594–598.

34 B. Febriansyah, C. S. D. Neo, D. Giovanni, S. Srivastava, Y. Lekina, T. M. Koh, Y. Li, Z. X. Shen, M. Asta, T. C. Sum, N. Mathews and J. England, Targeted Synthesis of Trimeric Organic-Bromoplumbate Hybrids That Display Intrinsic Highly Stokes-Shifted, Broadband Emission, *Chem. Mater.*, 2020, **32**, 4431–4441.

35 D. Tian, Z. Lai, H. Xu, F. Lin, Y. Jiang, Y. Huang, S. Wang, Y. Cai, J. Jin, R. J. Xie and X. Chen, Low-Dimensional Organic Lead Halides with Organic-Inorganic Collaborative Luminescence Regulated by Anion in Dimension, *Chem. Mater.*, 2022, **34**, 5224–5231.

36 Y. Takeoka, K. Asai, M. Rikukawa and K. Sanui, Hydrothermal Synthesis and Structure of Zero-Dimensional Organic-Inorganic Perovskites, *Chem. Lett.*, 2005, **34**, 602–603.

37 G. M. Sheldrick, SHELXT - Integrated Space-Group and Crystal-Structure Determination, *Acta Crystallogr., Sect. A: Found. Adv.*, 2015, **71**, 3–8.

38 G. M. Sheldrick, Crystal Structure Refinement with SHELXL, *Acta Crystallogr., Sect. C: Struct. Chem.*, 2015, **71**, 3–8.

39 C. K. N. Moller, On the structure of caesium hexahalogenoplumbates(II), *Mat. Fys. Medd. Dan. Vid. Selsk.*, 1960, **32**, 1–13.

40 R. H. Andrews, S. J. Clark, J. D. Donaldson, J. C. Dewan and J. Silver, Solid-State Properties of Materials of the Type Cs_4MX_6 (where M = Sn or Pb and X=Cl or Br), *J. Chem. Soc., Dalton Trans.*, 1983, 767–770.

41 K. Nitsch, M. Dousek, M. Nikl, K. Polak and M. Rodova, Ternary Alkali Lead Chlorides: Crystal Growth, Crystal Structure, Absorption and Emission Properties, *Prog. Cryst. Growth Charact. Mater.*, 1995, **30**, 1–22.

42 M. Mączka, J. Zienkiewicz and M. Ptak, Comparative Studies of Phonon Properties of Three-Dimensional Hybrid Organic–Inorganic Perovskites Comprising Methylhydrazinium, Methylammonium, and Formamidinium Cations, *J. Phys. Chem. C*, 2022, **126**, 4048–4056.

43 M. Mączka and M. Ptak, Lattice Dynamics and Structural Phase Transitions in Two-Dimensional Ferroelectric Methylhydrazinium Lead Bromide Investigated Using Raman and IR Spectroscopy, *J. Phys. Chem. C*, 2022, **126**, 7991–7998.

44 M. Mączka, S. Sobczak, P. Ratajczyk, F. F. Leite, W. Paraguassu, F. Dybała, A. P. Herman, R. Kudrawiec and A. Katrusiak, Pressure-Driven Phase Transition in Two-Dimensional Perovskite MHy_2PbBr_4, *Chem. Mater.*, 2022, **34**, 7867–7877.

45 D. Drozdowski, A. Gągor and M. Mączka, Methylhydrazinium Lead Iodide – One Dimensional Chain Phase with Excitonic Absorption and Large Energy Band Gap, *J. Mol. Struct.*, 2022, **1249**, 131660.

46 M. Mączka, M. Ptak, A. Gagor, D. Stefańska and A. Sieradzki, Layered Lead Iodide of $[Methylhydrazinium]_2PbI_4$ with a Reduced Band Gap: Thermochromic Luminescence and Switchable Dielectric Properties Triggered by Structural Phase Transitions, *Chem. Mater.*, 2019, **31**, 8563–8575.

47 K. Fedoruk, D. Drozdowski, M. Mączka, J. K. Zaręba, D. Stefańska, A. Gągor and A. Sieradzki, [Methylhydrazinium]$_2$PbCl$_4$, a Two-Dimensional Perovskite with Polar and Modulated Phases, *Inorg. Chem.*, 2022, **61**, 15520–15531.

48 Z. Zhang, Y. Zhu, W. Wang, W. Zheng, R. Lin, X. Li, H. Zhang, D. Zhong and F. Huang, Aqueous Solution Growth of Milimiter-Sized Nongreen-Luminescent Wide Bandgap Cs_4PbBr_6 Bulk Crystal, *Cryst. Growth Des.*, 2018, **18**, 6393–6398.

49 X. Chen, F. Zhang, Y. Ge, L. Shi, S. Huang, J. Tang, Z. Lv, L. Zhang, B. Zou and H. Zhong, Centimeter-Sized Cs_4PbBr_4 Crystals with Embedded $CsPbBr_3$ Nanocrystals Showing Superior Photoluminescence: Nonstoichiometry Induced Transformation and Light-Emitting Applications, *Adv. Funct. Mater.*, 2018, **28**, 1706567.

50 K. A. Akkerman, S. Park, E. Radicchi, F. Nunzi, E. Mosconi, F. De Angelis, R. Brescia, P. Rastogi, M. Prato and L. Manna, Nearly Monodispersed insulator Cs_4PbX_6 (X=Cl, Br, I) Nanocrystals, Their Mixed Halide Compositions, and Their Transformation into $CsPbX_3$ Nanocrystals, *Nano Lett.*, 2017, **17**, 1924–1930.

51 O. I. Yunakova, V. K. Miloslavskii and E. N. Kovalenko, Exciton Absorption Spectrum of Thin CsPbI3 and Cs4PbI6 Films, *Opt. Spectrosc.*, 2012, **112**, 91–96.

52 C. Ji, S. Wang, L. Li, Z. Sun, M. Hong and J. Luo, The First 2D Hybrid Perovskite Ferroelectric Showing Broadband White-Light Emission with High Color Rendering Index, *Adv. Funct. Mater.*, 2018, **29**, 1805038.

53 B. A. H. Huisman, F. Palazon and H. J. Bolink, Zero-Dimensional Hybrid Organic-Inorganic Lead Halides and Their Post-Synthesis Reversible Transformation into Three-Dimensional Perovskites, *Inorg. Chem.*, 2021, **60**, 5212–5216.

54 H. Gu, J. Xia, C. Liang, Y. Chen, W. Huang and G. Xing, Phase-Pure Two-Dimensional Layered Perovskite Thin Films, *Nat. Rev. Mater.*, 2023, **8**, 533–551.

55 Z. Zhang, J. F. Liao and G. Xing, Regulating the Coordination Geometry of Polyhedra in Zero-Dimensional Metal Halides for Tunable Emission, *Nanaoscale*, 2023, **15**, 5241–5248.

56 J. F. Liao, Z. Zhang, B. Wang, Z. Tang and G. Xing, Full-Color-Tunable Phosphorescence of Antimony-Doped Lead Halide Single Crystal, *npj Flexible Electron.*, 2022, **6**, 57.

57 S. K. Sharma, C. Phadnis, T. K. Das, A. Kumar, B. Kavaipatti, A. Chowdhury and A. Yella, Reversible Dimensionality Tuning of Hybrid Perovskites with Humidity: Visualisation and Application to Stable Solar Cells, *Chem. Mater.*, 2019, **31**, 3111–3117.

58 X. Li, S. A. Cuthriell, A. Bergonzoni, H. Dong, B. Traore, C. C. Stoumpos, P. Guo, J. Even, C. Katan, R. D. Schaller and M. G. Kanatzidis, Expanding the Cage of 2D Bromide Perovskites by Large A-Site Cations, *Chem. Mater.*, 2022, **34**, 1132–1142.

